Pulling-force-induced elongation and alignment effects on entanglement and knotting characteristics of linear polymers in a melt

E. Panagiotou[1,*] and M. Kröger[2,†]
[1]*Department of Mathematics, University of California, Santa Barbara, California 93106, USA*
[2]*Polymer Physics, Department of Materials, ETH Zurich, CH-8093 Zurich, Switzerland*
(Received 12 March 2014; revised manuscript received 5 July 2014; published 23 October 2014)

We employ a primitive path (PP) algorithm and the Gauss linking integral to study the degree of entanglement and knotting characteristics of linear polymer model chains in a melt under the action of a constant pulling force applied to selected chain ends. Our results for the amount of entanglement, the linking number, the average crossing number, the writhe of the chains and their PPs and the writhe of the entanglement strands all suggest a different response at the length scale of entanglement strands than that of the chains themselves and of the corresponding PPs. Our findings indicate that the chains first stretch at the level of entanglement strands and next the PP (tube) gets oriented with the "flow." These two phases of the extension and alignment of the chains coincide with two phases related to the disentanglement of the chains. Soon after the onset of external force the PPs attain a more entangled conformation, and the number of nontrivially linked end-to-end closed chains increases. Next, the chains disentangle continuously to attain an almost unentangled conformation. Using the linking matrix of the chains in the melt, we furthermore show that these phases are accompanied by a different scaling of the homogeneity of the global entanglement in the system. The homogeneity of the end-to-end closed chains first increases to a maximum and then decreases slowly to a value characterizing a completely unlinked system.

DOI: 10.1103/PhysRevE.90.042602 PACS number(s): 83.80.Sg, 02.10.Kn, 83.10.Kn, 05.40.Fb

I. INTRODUCTION

Polymer melts solely composed of macromolecules exhibit time-dependent mechanical properties, termed viscoelastic because of the combination of viscous flow at long times and elastic response at short times. Beyond the linear flow regime, a variety of structural, rheological, and topological properties are found to display significant deviations from their corresponding equilibrium behaviors [1–3]. Presently, nonequilibrium viscoelastic processing flows cannot be easily characterized (or even formulated) within one macroscopic model due to the myriad of relaxation phenomena occurring at multiple length and time scales within these materials [4,5]. Given that polymer chains cannot cross each other, dynamics in entangled polymers differ substantially compared to unentangled systems due to the existence of topological interactions dominating their rheological behavior [6]. A fundamental understanding of the entanglement relaxation mechanisms and phenomena occurring across these scales is thus a prerequisite for predicting the response of these systems to an applied flow field [7–13].

Edwards [1] suggested that entanglements effectively restrict individual chain conformations in a curvilinear tubelike region enclosing each chain [14]. At very short time scales, chain segments are allowed to freely fluctuate in all directions until their displacements become commensurate with the tube diameter, which is the end-to-end distance of a portion of the polymer chain, called the *entanglement strand*. The axis of the tube is a coarse-grained representation of the chain and it is called the *primitive path* (PP). Several methods have been developed for extracting the PP network [15–21]. Two geometrical methods capable of efficiently reducing computer generated polymer models to entanglement networks are the Z1 code [16,18,22,23] and the CReTA algorithm [17]. Despite differences in their specific implementation, these methods are reported to yield similar results for the average properties of the PP network [16–18,24–29]. The nonlinear rheological behavior of polymer chains in flow can be understood in terms of yielding through disintegration of the chain entanglement network. Therefore it is interesting to understand how the entanglement network deforms with the test chain under the influence of a strong deformation [5,8–11,13,21,30–35].

Under certain conditions, we can see the polymer chains as simple mathematical curves in space. A *knot* (respectively, *link*) is one (or more, respectively) simple closed curve(s) in space without intersections. It has been shown [36] that knots slow down the stretching of individual polymers. The complexity (or topological state) of these knots or links is related to their global entanglement and it can be measured by using *topological invariants* such as knot or link polynomials [37–39]. The topological invariants are properties of knots or links, which remain invariant for isotopic configurations. In the case of linear polymers, the notion of topological invariant does not apply, since linear chains can be continuously deformed to attain any configuration, as noted earlier [14,40]. Efforts have been made to characterize the knotting of an open chain [41–45]. A measure of entanglement that is meaningful both for closed or open chains is the *Gauss linking integral* [40]. For two closed chains (ring polymers) the Gauss linking integral is a topological invariant that measures the algebraic number of times one chain turns around the other. For two open chains (linear polymers), it is a real number that is a continuous function of the chain coordinates. The Gauss linking integral can be also applied to one chain in order to provide measures of self-entanglement of a chain, called *writhe* [46–51] and *average crossing number* [47,52–55]. These are real numbers

*Corresponding author: panagiotou@math.ucsb.edu
†http://www.complexfluids.ethz.ch

that change continuously under continuous deformations of a chain. Thus, the writhe and the average crossing number are very clearly not topological invariants, even for closed chains, but, rather, they are quantities that depend on the specific geometry of the chain, and are very sensitive to the specific conformations that are analyzed.

In this work we study the entanglement characteristics of linear chains in a melt under the action of directed forces by combining the entanglement network properties with tools from knot theory. We obtain information about the motion of the chains, their PPs, and the entanglement strands. We consider therefore this work as a step towards a more comprehensive understanding of the topological interaction of a polymer melt with a flow, a very complicated problem including among others poorly understood components today, such as what is the role of molecular architecture [56,57] and the role of embedded nanoparticles [58,59]. The setup employed in this work could represent future experiments involving magnetic nanoparticles attached to terminal monomers [60–64].

More precisely, in Sec. II we describe the measures of entanglement used in this study. In Sec. III we describe the simulation method used to sample a polymer melt of linear finitely extendable nonlinear elastic (FENE) multibead chains under the action of pulling forces. In Sec. IV the results on the PP network characteristics obtained by the Z1 algorithm, the average crossing number, the writhe of the original FENE chains, the Z1-reduced chains, the entanglement strands, and the linking number and the *linking matrix* of the chains are presented and analyzed.

II. MEASURES OF ENTANGLEMENT

A. Z1 algorithm

The Z1 algorithm [22] is a state-of-the-art geometric algorithm which proceeds by transforming the physical picture of topological interchain constraints as conceived by Doi and Edwards [1] into a pure mathematical problem of identifying the shortest multiple disconnected (primitive) path subject to geometrical constraints arising from the configuration of the corresponding atomistic system. More precisely, given a polymer melt configuration, the algorithm minimizes the total contour length of all chains, while all chain ends remain fixed in space, by moving the beads sequentially in space while maintaining the noncrossability of the chains. In this way the chains become rectilinear strands coming together at kinks where the entanglements occur. Unphysical disentanglement is prevented by constraining moves of kinks to lie in the plane of their adjacent segments [16]. In this study, to allow for a direct comparison with previous works [65], we use the version of Z1 that does not capture self-entanglements. One has to be aware that even if self-crossings are allowed (which are rare [24]), the global self-entanglement remains, due to the uncrossability with other chains.

A direct consequence of the specific mathematical formulation is that the Z1 algorithm provides as output the average contour length of a PP, $\langle L_{\mathrm{PP}}\rangle$. The probability distribution of L_{PP} is practically Gaussian. Here and in the following, $\langle\,\rangle$ denotes averaging over all chains of a given configuration. In addition, by mapping the extracted interior nodes of each PP into kinks, the average number of interior kinks (entanglements), $\langle Z\rangle$, per chain is returned. The probability distribution of $\langle Z\rangle$ has been approximated by a Poissonian [27,66–68]. We will use the following notation for the average values of these quantities over all chains: $\mathcal{Z} = \langle Z\rangle$ and $\mathcal{L}_{\mathrm{PP}} = \langle L_{\mathrm{PP}}\rangle$. Finally, from the output of Z1 one can recover entanglement molecular weights (N_e) in accordance with experiments [65].

B. The Gauss linking integral

The Gauss *linking number* L of two oriented curves l_1 and l_2, whose arc-length parametrizations are $\gamma_1(t)$ and $\gamma_2(s)$, respectively, is defined as a double integral over l_1 and l_2 [69]:

$$L(l_1,l_2) = \frac{1}{4\pi}\int_{[0,1]}\int_{[0,1]} \frac{(\dot\gamma_1(t),\dot\gamma_2(s),\gamma_1(t)-\gamma_2(s))}{|\gamma_1(t)-\gamma_2(s)|^3}\,dtds, \tag{1}$$

where $(\dot\gamma_1(t),\dot\gamma_2(s),\gamma_1(t)-\gamma_2(s)) = (\dot\gamma_1(t)\times\dot\gamma_2(s))\cdot(\gamma_1(t)-\gamma_2(s))$.

The *writhe* W of an oriented curve l with arc-length parametrization $\gamma(t)$ is thus alternatively and more conveniently defined by the Gauss linking integral over a curve

$$W(l) = \frac{1}{2\pi}\int_{[0,1]^*}\int_{[0,1]^*} \frac{(\dot\gamma(t),\dot\gamma(s),\gamma(t)-\gamma(s))}{|\gamma(t)-\gamma(s)|^3}\,dtds, \tag{2}$$

where $[0,1]^*\times[0,1]^* = \{(x,y)\in[0,1]\times[0,1]|x\neq y\}$.

The *average crossing number* (ACN) of a curve l, parameterized by $\gamma(t)$, is defined as

$$\mathrm{ACN}(l) = \frac{1}{2\pi}\int_0^1\int_0^1 \frac{|(\dot\gamma(t),\dot\gamma(s),\gamma(t)-\gamma(s))|}{|\gamma(t)-\gamma(s)|^3}dtds. \tag{3}$$

The geometrical meaning of the ACN, the writhe, and the linking number is the same for open or closed curves. Without loss of generality, we can assign an orientation to the chains. Then in a random projection direction one can see crossings of the type shown in Fig. 1. Then for one (respectively, two) oriented curve(s), the writhe (respectively, the linking number) is the average over all projection directions of the algebraic sum of crossings (or intercrossings, respectively), in the projection of the curve (or curves, respectively). Similarly, the ACN is the average sum of crossings (without signs) in a generic orthogonal projection over all possible projection directions. When applied to open chains all these measures are continuous functions in the space of configurations. Furthermore, as the end points of the curves move towards coincidence, these measures tend to their values for the resulting closed knots

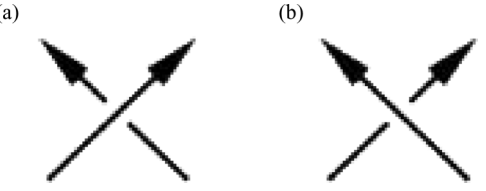

FIG. 1. (a) +1 crossing and (b) −1 crossing. By assigning a sign to each crossing, one recovers information concerning which arc comes over and under.

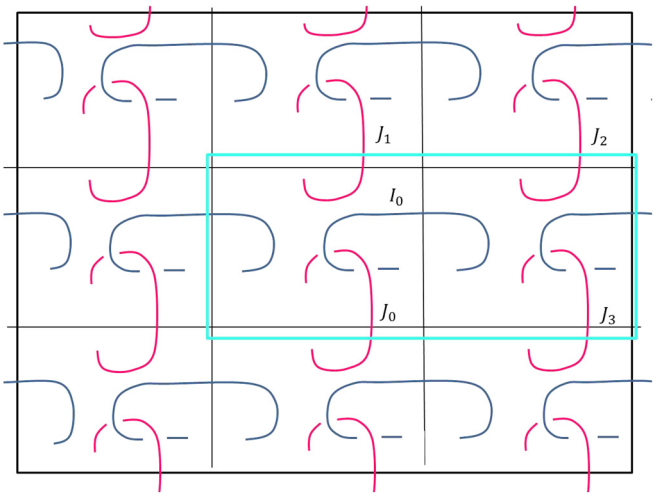

FIG. 2. (Color online) A system generated by two chains. For the computation of $\mathrm{LK}(I,J)$ we have $\mathrm{LK}(I,J) = L(I_0,J_0) + L(I_0,J_1) + L(I_0,J_2) + L(I_0,J_3)$.

or links. In the case of closed chains the linking number is a topological invariant.

In the following we will take averages of the ACN, the writhe, and the linking number of polymer chains in melts simulated with the use of a periodic box. The periodic box is replicated in space to form a large bulk system; we call it the *periodic system* [21,70,71]. For a system with M *generating chains* in a periodic box, there are only M different conformations in the periodic (bulk) system that the box generates and infinitely many *images* (i.e., copies) of these conformations (see Fig. 2 for an illustrative example). For measuring the mean values of the absolute writhe or the mean ACN of a chain in a system of M chains in a periodic box it suffices to measure the absolute writhe or the ACN of the M different unfoldings and divide by M, since there are only M different conformations.

In the case of the linking number, the situation is different, since there are infinitely many pairs of chains in the periodic system in different relative position [70,71]. Obviously, it does not make sense to compute the linking numbers of all the infinite numbers of different pairs of images in the periodic system. In [70] a new linking measure for chains in PBC was introduced—the *local periodic linking number*: For two simulation chains I,J, their local periodic linking number is equal to

$$\mathrm{LK}(I,J) = \sum_{u \in \mathrm{unf}(I_1)} L(I_1, J_u), \tag{4}$$

where J_u is an image of J that intersects the cells in which I_1 unfolds [we denote $u \in \mathrm{unf}(I_1)$]; see Fig. 2 . The local periodic linking number takes into account all the linking imposed to one chain in its vicinity by images of another chain with no repetitions. Also, this is independent of I_1, i.e., the same for all the images of I, and it is symmetric, i.e., $\mathrm{LK}(I,J) = \mathrm{LK}(J,I)$ [70].

Accordingly, for our estimation of the mean absolute linking number we take the average of all the absolute values of the linking numbers of the pairs of chains (I_1, J_u), $u \in \mathrm{unf}(I_1)$, for all pairs of generating chains I,J (i.e., the average of all summands in $\mathrm{LK}(I,J)$ of all possible pairs of generating chains).

C. The linking matrix

For measuring the homogeneity of the global entanglement in the system, we employ a measure of entanglement that takes into consideration all the global pairwise linking in the system. We define a linking matrix for a cell of n generating chains as the $n \times n$ matrix with components $\mathrm{LK}(I,J)$, the local periodic linking number of the I and J chain. The diagonal component $\mathrm{LK}(I,I)$ is the local periodic linking number of I with its own images [40,71].

We consider the absolute linking matrix as an adjacency matrix of a weighted graph whose vertices correspond to the generating chains and the weight of the edge that connects the ith and jth vertex is the local periodic linking number of the corresponding generating chains. Using tools from graph theory, such as the Cheeger constant, h_G, we can detect the expansion property of the graph, and use it as a measure of homogeneity of the global linking in the system [71]. This measure of entanglement does not provide information about the distribution of kinks in space, but it detects whether there are sets of chains highly linked with each other, and poorly linked with the chains in the complement of that set. A direct calculation of h_G is computationally expensive; below we instead report results for the second eigenvalue of the Laplacian of the absolute linking matrix, λ_2, which is related to the dimensionless Cheeger constant via the inequalities $2h_G \geqslant \lambda_2 \geqslant h_G^2/2$ [72]. Moreover, we present the maximum eigenvalue of the Laplacian, $\lambda_{\max}$, which has the property $\lambda_{\max} = 2$ if and only if G has a connected component that is bipartite and nontrivial.

III. SIMULATION METHOD

To study the pulling-force-induced flow behavior of model polymer melts, we have performed nonequilibrium molecular dynamics (NEMD) computer simulations at constant bead number density, volume, and temperature (NVT ensemble) in a cubic cell with periodic boundary conditions. More precisely, we study a classical multibead FENE chain system [73] with a dimensionless number density 0.84 at temperature $T = 1$, with $M = 100$ linear chains, where each chain consists of $N = 100$ beads. All the beads interact with a purely repulsive part of the Lennard-Jones potential, and all dimensionless values are given in Lennard-Jones (LJ) units involving the depth of the LJ potential ϵ, its characteristic length σ, and the bead mass m. All dimensionless numbers can be readily converted to dimensional numbers [74], since for any dimensional quantity Q_{phys} with SI units $[Q_{\mathrm{phys}}] = \mathrm{kg}^{\alpha}\ \mathrm{m}^{\beta}\ \mathrm{s}^{\gamma}$ one has $Q_{\mathrm{phys}} = Q \times Q_{\mathrm{ref}}$ with $Q_{\mathrm{ref}} = m^{\alpha+\gamma/2}\sigma^{\beta+\gamma}\epsilon^{-\gamma/2}$, and we mention dimensionless values Q throughout. For beads which are bonded neighbors along the chain (for $N > 1$), an attractive potential (FENE potential) is added. With the choice for the finite extensibility of the FENE spring, $R_0 = 1.5$ and $k^* = 30$, we follow previous investigations [73,75].

The simulation of elongational flow experiments in polymer melts usually involves a change of the shape of the periodic

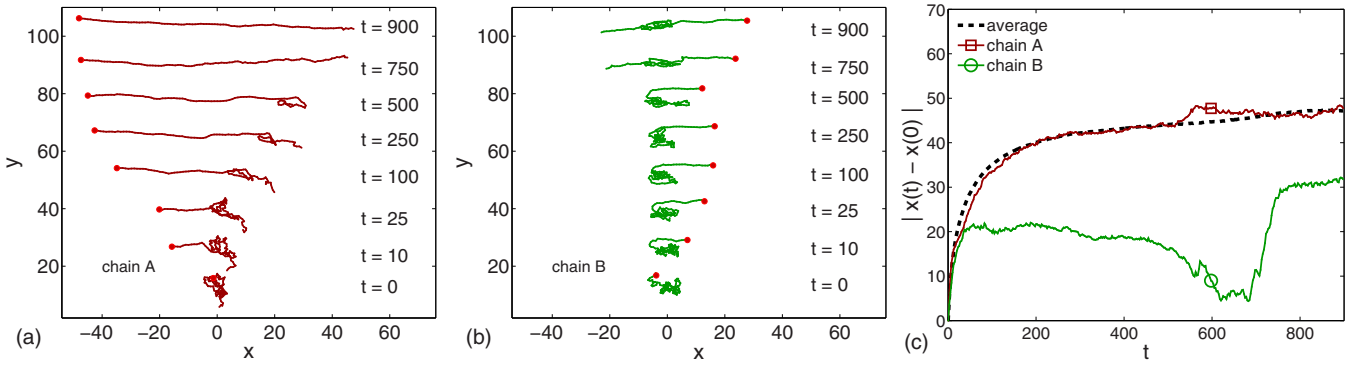

FIG. 3. (Color online) (a), (b) Selected sequences of snapshots for individual chains contained in the melt, artificially shifted vertically with time. The marked head groups experience a constant force in the x direction. Chains tend to either unravel completely (chain A, whose absolute writhe decreases from 2.246 to 0.130), or to tighten existing knots (chain B, whose $|W|$ increases from 0.237 to 0.820); the shrinkage in the y direction of not yet unfolded chain ends is caused by the invisible surrounding chains. The stretched terminal part containing the force-bearing end group is responsible for an initial increase of the number of entanglements, which are subsequently destroyed upon unraveling. (c) Absolute displacement of the force-bearing bead in the x direction for the two chains shown in (a) and (b), as well as $\langle|x(t) - x(0)|\rangle$ obtained as an average over all chains. The initial quick increase terminates when $\langle|x(t) - x(0)|\rangle$ exceeds 40, which corresponds to roughly half of the length of a stretched entanglement strand. This regime is followed by a regime of constant speed of the polymer's center of mass, $v = \langle|x(t) - x(0)|\rangle/t \approx 0.0078 = F/\zeta N^2$ with $\zeta \approx 0.64$ reflecting Stokes friction.

box. The change of the shape of the simulation cell affects the periodic structure of the system. As has been pointed out in previous studies [21,70,71], the periodicity of the system affects the entanglement of the chains. Here, we are interested in the changes of the entanglement characteristics of the system due to the alignment of the chains. Thus, to reduce the effect of the change of the periodicity of the system on the entanglement of the chains, we choose to make simulations where the shape (and the size) of the simulation cell are fixed.

To create samples that largely differ in their number of entanglements, while N and the simulation box size remain constant, we apply a constant force of magnitude $F = 50$ pointing into the negative (positive) x direction to all those terminal beads (a randomly selected one for each chain) that are initially located in the left (right) half of the simulation box. We use a time step $\Delta t = 0.005$ and configurations are kept each 50 iterations. The bond lengths fluctuate between 0.6 and 1.45 during such runs, and since the Boltzmann weight related to the LJ potential evaluated at $R_0/2$ is about $\exp(-100/T) \approx 10^{-44}$, it is practically impossible for chains to slip through each other. Periodic boundary conditions are applied during all the simulations to the simulation box of fixed size; the monomer density thus remains constant.

With time the chains tend to be pulled straight (while remaining within the periodic simulation box) as a result of the enforced overall deterministic motion of their selected ends (Figs. 3 and 4). Thus, the simulated system gives insight to the situation where the sample is deformed at an increasing rate in the x direction. A peculiarity of this simulation setup is that one can reach a state of almost fully elongated chains, while going through all intermediate states of partial elongation quickly compared with the situation encountered in conventional elongational flows, where the flow-induced alignment is caused by thermostatting with respect to an affine deformation. Still, the corresponding experiment could in principle be performed with linear polymers subjected to electromagnetic fields, which carry single molecule magnetic or charged particles or optical tweezers at their end groups [77,78], while experiments involving such nanoparticles are also of biomedical interest [60–64].

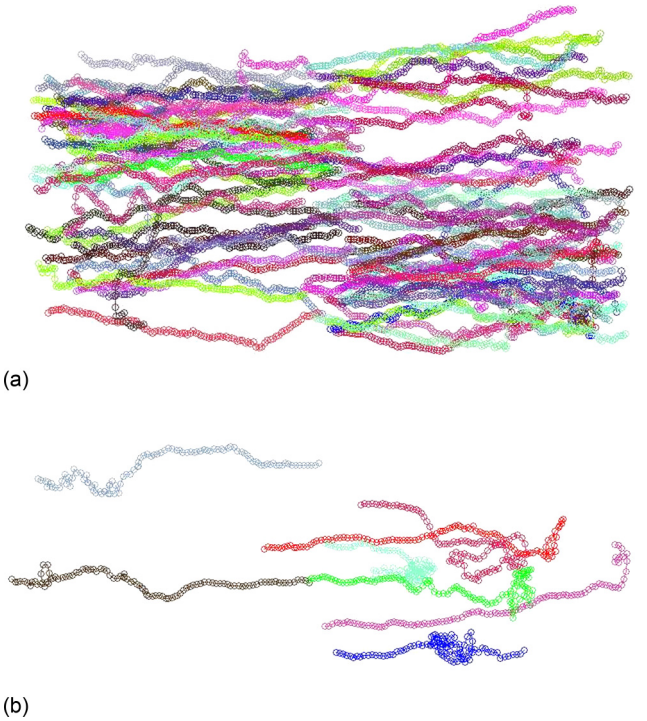

FIG. 4. (Color online) Visualization of the final elongated melt state. Only the parent images of the total 100 chains are shown. Subset of chains with (a) $|W| < 0.5$ and (b) $|W| \geqslant 0.5$. As expected, most of the chains with $|W| > 0.5$ contain local tight knots [76].

IV. RESULTS AND DISCUSSION

We aim at characterizing the entanglement of a polymer melt sample of linear chains under the influence of external pulling forces, as already described. By analyzing the results obtained by the Z1 algorithm, the ACN, the writhe, and the linking number of the chains in time, we provide information on the entanglement and the motion of the chains, the tube, and the entanglement strands. Later below we use the linking matrix to extract information concerning the global pairwise homogeneity of the entanglement in the system.

A. The end-to-end distance

We first examine the end-to-end distance of the chains, R_{ee}, which serves as a simple indicator for the elongation of the chains. There have been three main models proposed for the end-to-end distance of the chains in classical elongational flow. First, King and James [79] proposed that in transient flow, polymer chains "freeze" in partially extended conformations, because of the presence of self-entanglements or knots. This implies a very slow and nonaffine response. Next, Ryskin [80] suggested that in a supercritical flow the chain is stretched near the center of the molecule and curled up at the ends. In this model a nearly affine response should prevail until the molecule is nearly fully extended. Finally, Rallison and Hinch [31] and Larson [32] observed that soon after onset of a strong elongational flow, the polymer molecule is driven into a highly folded or kinked state which suggests that the response might be affine until the chain is stretched to perhaps five times its equilibrium length and thereafter the chain might stretch at perhaps one-third the flow rate of the solvent, also supported by experimental studies [6]. Our results indicate a behavior similar to the latter.

Figure 5(a) shows $\mathcal{R}_{ee} = \langle R_{ee}^2 \rangle^{1/2}$ as a function of time. The plateau value is $\mathcal{R}_{ee} \approx 93$, i.e., $\sim 93\%$ of the value corresponding to the fully aligned conformation whose bonds remain at the equilibrium bond length ≈ 1. The behavior is in qualitative agreement with other simulations and experiments of chains subjected to flow where it is attributed to chain rotation, tumbling, and flow alignment under shear or elongation [13,33,34,73,81–85], while the force-induced pulling does not give rise to tumbling or rotation except partially in a very early stage of disentanglement. We observe that $\mathcal{R}_{ee}$ initially increases rapidly with time, in analogy to the case of an applied shear or elongational flow. A simultaneous chain alignment is visually obvious from the snapshots in Figs. 3 and 4. Up to $\mathcal{R}_{ee} \approx 60$ ($t \leqslant 150$) the end-to-end distance shows an affine increase. This time is small compared with the longest relaxation time $\tau \approx 0.39N^2 + 0.005N^3 \approx 0.39[1 + (N/78)]N^2 \approx 8900$ of our FENE polymer melt chains, according to [10]. Next, a transition to a nonaffine transformation occurs and the increase in the chain dimensions gradually slows down leading eventually to the plateau. The slowing down of the increase of the end-to-end distance may be due to the increasing effect of intermolecular collisions [34], and also due to the existence of knotted configurations [36]. Figure 5(b) shows the double logarithmic plot of $\mathcal{R}_{ee}$ versus t. We observe that $\mathcal{R}_{ee}$ is approximately constant for $t < 10$, as expected, since a polymer under tension begins to deform when the force due to hydrodynamic friction across the molecule exceeds the entropic elasticity that tends to coil it [6].

B. The number of entanglements per chain

In this paragraph we discuss the transient behavior of the PP network during elongation as it is captured by the Z1 algorithm. Figure 6(a) shows the mean number of kinks $\mathcal{Z}$ as a function of time, where a decrease of $\mathcal{Z}$ signals a disentanglement process. The initial value of $\mathcal{Z}$ at $t = 0$ for the sample under consideration is approximately $\mathcal{Z}(0) \approx 2.2$, which is in accordance with values obtained in previous studies for the same systems in equilibrium [14]. For $t < 8$ the number of entanglements remains almost constant around its equilibrium value. For $t < 150$, $\mathcal{Z}$ increases monotonically up to $\mathcal{Z}(150) \approx 5.3$. Next $\mathcal{Z}$ decreases and we observe a change of slope at $t \approx 450$. Notice that $\mathcal{Z}(450) \approx \mathcal{Z}(0)$ indicating that the extra entanglements are lost. Later on, $\mathcal{Z}$ continues to decrease and we observe a change of slope at $t \approx 600$. We find $\mathcal{Z}(600) \approx 1$, suggesting that at $t > 600$ the chains have disentangled completely, while $\mathcal{Z} = 0$ corresponds to a system of perfectly rodlike chains.

Thus, we have observed four phases which can be described also as (1) creation of extra entanglements, (2) loss of extra entanglements, (3) disentanglement of original entanglements, and (4) loss of all entanglements. The duration over which $\mathcal{Z}$ initially increases seems to coincide with that of the affine increase of the end-to-end distance, while a perfectly affine deformation of the configuration should not alter the amount of entanglement. Figure 6(b) shows the double logarithmic plot of $\mathcal{Z}$ versus t. There is one crossover at $t \approx 150$ and

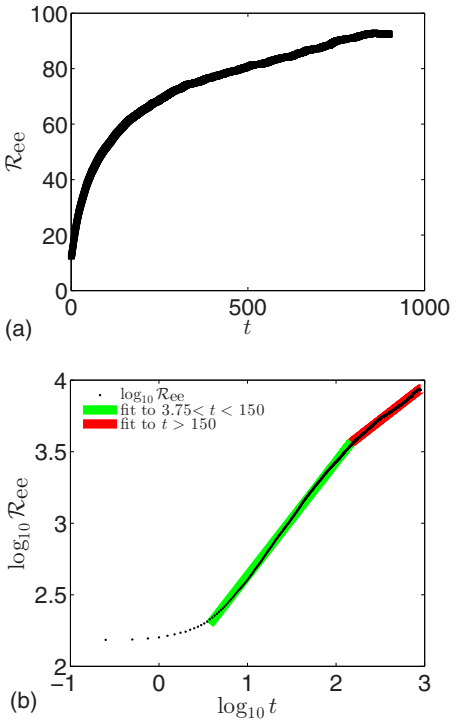

FIG. 5. (Color online) (a) Square root of the mean squared end-to-end distance, $\mathcal{R}_{ee} = \langle R_{ee}^2 \rangle^{1/2}$, as a function of time. (b) The corresponding double logarithmic plot.

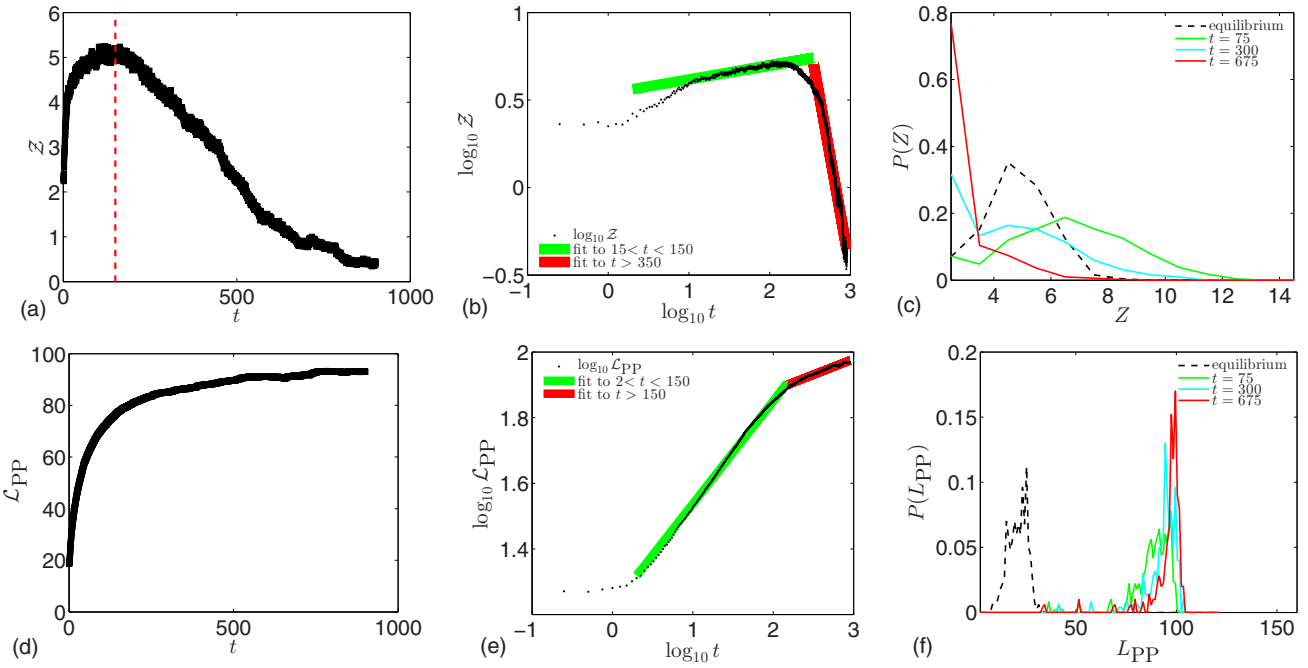

FIG. 6. (Color online) (a) Number of entanglements computed by the Z1 algorithm. The vertical dashed line is at $t = 150$. (b) Double logarithmic plot of $\mathcal{Z} = \langle Z \rangle$ with t. (c) Probability distribution of Z in the course of time. (d) Average contour length of the PP, $\mathcal{L}_{\rm PP} = \langle L_{\rm PP} \rangle$. (e) Double logarithmic plot of $\mathcal{L}_{\rm PP}$ vs t. (f) Probability distribution of $L_{\rm PP}$ in the course of time.

eventually a second one at $t \approx 450$. We note that at $t < 3$, the degree of entanglement is almost constant, in agreement with the results on $\mathcal{R}_{\rm ee}$. At $3 < t < 25$, $\mathcal{Z}$ increases and its increase slows down at $25 < t < 150$.

The increase of $\mathcal{Z}$ is a surprising result since one expects that the network will disentangle as the chains stretch in time [34]. This has been observed also before for knotted configurations [36]. The excess in $\mathcal{Z}$ may be an effect of the particular protocol, where the chain ends are pulled into the initially stationary matrix of the other chains and, thus, as the chains stretch out, there is more available length where contacts with other chains can occur (Figs. 3 and 4). On the other hand, this transient increase of entanglement correlates with the overshoot of the viscosity in elongational flows [86], and we expect the overshoot to be less dominant at smaller force strengths. Rallison and Hinch [31] showed that a polymer of modest to high molecular weight in a strong extensional flow collapses within about three Hencky strain units to a kinked state with a few to a few hundred kinks, due to the slow unfolding of back-loops [32]. Such back-loops, characterized by strong alignment, but incomplete extension, may contribute to the overshoot.

Our NEMD results for the probability distribution of $P(Z)$ of the number of entanglements as a function of time is shown in Fig. 6(c). At equilibrium, the distribution is Poissonian (very similar to the Gaussian one for large values of the mean), which is consistent with previous analysis of linear polymer melts [4,33]. As the time increases, the $P(Z)$ curves are seen to move to larger $\mathcal{Z}$ values characteristic of more and more entanglements per chain. As the elongation time is increased even further, the $P(Z)$ curves seem to move to smaller $\mathcal{Z}$ values characteristic of less and less entanglements per chain. At $t \approx 675$, $P(Z)$ attains a non-negligible value for $\mathcal{Z} < 1$, revealing the existence of chains completely devoid of entanglements. This indicates that at high elongation rates a significant number of chains are not entangled with other chains, which in turn implies chains with a collapsed overall structure.

C. The PP contour length

Figures 6(d)–6(f) show $L_{\rm PP}$ and its distribution in time as it is computed by the application of the Z1 algorithm. Note that it was observed that $\mathcal{L}_{\rm PP}$ mirrors the behavior of the intramolecular LJ energy [34]. We observe that the quantity increases rapidly with time in accordance with previous studies of similar systems [33,34]. For our system, however, this scaling is surprising when compared to the behavior of $\mathcal{Z}$ which is not monotonic. This suggests that even though both $\mathcal{Z}$ and $\mathcal{L}_{\rm PP}$ are calculated by the reduced network and concern entanglement information per chain, they provide complementary information.

We observe a similarity between the behavior of $\mathcal{L}_{\rm PP}$, the mean contour length of the PPs, and that of their end-to-end distance $\mathcal{R}_{\rm ee}$, while the two measures certainly do not capture the same information (Fig. 7). For $t < 600$, $\mathcal{L}_{\rm PP}$ increases monotonically, changing slope at $t \approx 150$. For $t < 150$, $\mathcal{L}_{\rm PP}$ increases at a rate larger than that of $\mathcal{R}_{\rm ee}$. This happens because for $t < 150$, both $\mathcal{Z}$ and $\mathcal{R}_{\rm ee}$ increase as well. For $t > 150$ there are two competing effects: the increase of the chain dimensions which tends to increase $L_{\rm PP}$ and the decrease in the degree of topological interactions as the chains are aligned more and more with the flow which tends to decrease $\mathcal{L}_{\rm PP}$. We observe that for $t > 150$, $\mathcal{L}_{\rm PP}$ increases, thus chain stretching is more pronounced than the loss of entanglements. Note that the plateau value for $\mathcal{L}_{\rm PP}$ is $\mathcal{L}_{\rm PP} \approx 93 \approx \mathcal{R}_{\rm ee}$, which indicates that there are almost no entanglements at large t, as expected.

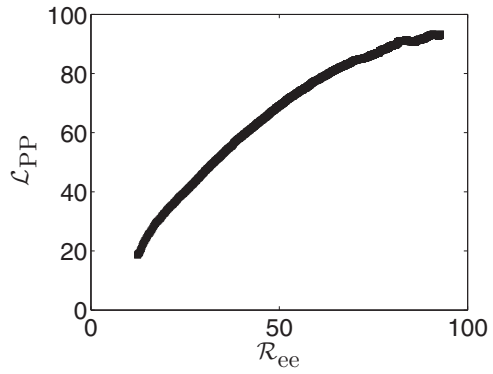

FIG. 7. The mean primitive path contour length, $\mathcal{L}_{PP}$, versus the square root of the mean squared end-to-end distance, $\mathcal{R}_{ee}$.

However, while the asymptotic value of $\mathcal{R}_{ee}$ is approximately nine times larger than the equilibrium one, the maximum value of $\mathcal{L}_{PP}$ is only at about 4.5 times larger than the corresponding equilibrium value. Similar results were observed in [33] and it is understood that the assumed increase in $\mathcal{L}_{PP}$ associated with the increase in $\mathcal{R}_{ee}$ is largely compensated by the loss of topological interactions due to chain alignment.

At equilibrium the probability distribution of L_{PP} [Fig. 6(f)] is practically Gaussian. The distribution shifts to the right indicating relatively higher L_{PP} values compared to those in equilibrium. As time increases, the distribution becomes increasingly asymmetric with respect to its most probable value suggesting significant variations from the Gaussian shape. A qualitatively similar trend had been reported for the case of shear flow [33], where the asymmetry appears more gradually.

D. The length of an entanglement strand

It had been repeatedly suggested that the tube diameter and distance between entanglements should be affected by deformation [11]. Accordingly, one expects that as the chains disentangle the tube diameter increases. Within this picture the average number of monomers in an entanglement strand, i.e., the entanglement length, denoted N_e, increases as well. During the deformation protocol used here initial random walk conformations are transformed into extended, rodlike conformations; a meaningful N_e estimator has to get both the coil and rod limits correctly, and to be able to predict stress relaxation, e.g., due to convective constraint release [87,88]. The Z1 code returns for each chain value for Z, L_{PP}, and R_{ee}, by which various N_e estimators, denoted $\mathcal{N}_e(N)$, can be computed [65]. Their interpretation for the case of a nonequilibrium situation had not yet been explored in the literature, with one exception that concerns the degree of entanglement in the presence of confinement [89].

There are estimators derived from moments of the distributions of L_{PP} and R_{ee} values based on a consideration of the PP as a random coil. These are the classical *S-coil* estimator

$$\mathcal{N}_e(N)^{\text{S-coil}} = (N-1)\frac{\langle R_{ee}^2\rangle}{\langle L_{PP}\rangle^2}, \tag{5}$$

and the *modified S-coil* estimator

$$\mathcal{N}_e(N)^{\text{modS-coil}} = (N-1)\left(\frac{\langle L_{PP}^2\rangle}{\langle R_{ee}^2\rangle} - 1\right)^{-1}. \tag{6}$$

There are also estimators based on $\mathcal{Z}$, such as the classical *S-kink* estimator

$$\mathcal{N}_e(N)^{\text{S-kink}} = \frac{N(N-1)}{\mathcal{Z}(N-1)+N}, \tag{7}$$

and the *modified S-kink* estimator

$$\mathcal{N}_e(N)^{\text{modS-kink}} = \frac{N}{\mathcal{Z}}. \tag{8}$$

In [14] a new N_e estimator was introduced for semiflexible chains of equilibrium stiffness parameter κ (related to persistence length), as

$$\mathcal{W}_e^2 = 0.029\,19\left(\frac{\mathcal{N}_e}{\kappa}\right)^{1.18}, \tag{9}$$

where $\mathcal{W}_e^2$ denotes the mean squared writhe of an entanglement strand. In the nonequilibrium situation where the chains get distorted due to the pulling force, they no longer behave like semiflexible chains of a constant stiffness parameter $\kappa = 2.34$ in equilibrium [14]. The discrepancy is caused by the polymer chains that are increasingly stretched and aligned during the pulling experiment. The chains locally stiffen in the course of time. A nonequilibrium analog to κ related to the average scalar product between adjacent bond vectors $\mathbf{u}_i$ and $\mathbf{u}_{i+1}$, $\kappa(t) \approx \frac{1}{2} - 1/\ln\langle \mathbf{u}_i \cdot \mathbf{u}_{i+1}\rangle$ could be used in Eq. (9) to capture this effect. The analysis of κ on our data shows that it basically linearly increases up to $\kappa \approx 20$ at $t = 900$.

Note that the estimators based on $\mathcal{Z}$ are also called *topological estimators*, while the estimators based on L_{PP} are sometimes called *plateau estimators* or *coil estimators* (more counterintuitively also termed *rheological estimators*) to highlight the fact that the two give different results and that the plateau estimators had been shown to be in good agreement with experimental values of the entanglement length contained in the plateau modulus for equilibrium systems [90]. The classical coil and kink estimators all identify straight PP sections with entanglement strands. This remains, of course, an unproven simplification and it has been shown that there are numerical prefactors between the number of monomers in an entanglement strand, and the corresponding plateau modulus, i.e., the length scale where topological effects of entanglements are felt [90]. The estimator based on writhe and $\mathcal{Z}$ has the advantage that it does not depend directly on the exact locations where the kinks occur, nor on the value of L_{PP}. For systems in equilibrium, this estimator gives values between the kink and coil estimators, and is in good agreement with experimental data on N_e, i.e., it is a good approximation of the rheological entanglement length [90].

Results for all four classical N_e estimators, when applied to a nonequilibrium situation, are shown in Fig. 8. Except at $t = 0$, these estimators do not provide a measure for an equilibrium N_e. Apparently, the estimators based on kinks and on coils give different results at each time with the latter being almost twice as large as the former. This suggests that the "topological" and "rheological" estimators are roughly proportional to each other also in the present nonequilibrium situation, while it is

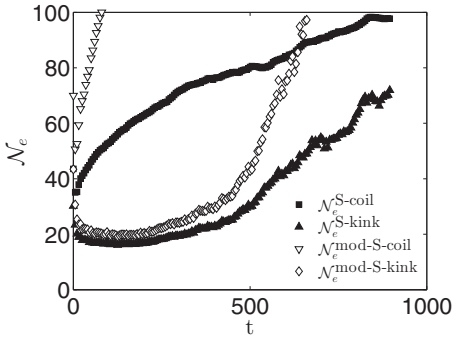

FIG. 8. N_e estimators: $\mathcal{N}_e^{\text{S-coil}}$, $\mathcal{N}_e^{\text{S-kink}}$, $\mathcal{N}_e^{\text{mod S-coil}}$, $\mathcal{N}_e^{\text{mod S-kink}}$ defined in Eqs. (5)–(8). The latter two estimators exceed $N = 100$ at large times. Values for all four estimators in equilibrium ($t = 0$) had been obtained for a large set of initial configurations in [65].

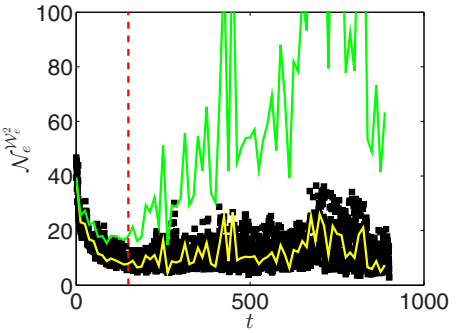

FIG. 9. (Color online) The entanglement length as obtained by the estimator involving the writhe and $\mathcal{Z}$, Eq. (9), using the equilibrium value $\kappa = 2.34$ (black data points). The yellow line is a smoothed version of the data (averaged over $\Delta t = 50$) and the green line shows the values of the N_e estimator obtained using the measured nonequilibrium analog to bending stiffness, $\kappa(t) = 2.34 + 0.02\,t$ in Eq. (9). The estimator gives values intermediate between the $\mathcal{N}_e^{\text{S-coil}}$ and $\mathcal{N}_e^{\text{S-kink}}$ estimators (Fig. 8), but shows also a jump to values greater than 100 at about $t \approx 450$.

obvious that the assumptions underlying the definition of N_e from coils must fail in an anisotropic situation. Still, due to the relevance of the coil picture in the literature and for a complete comparison of the equilibrium results we have chosen to present results for the coil estimators as well. The modified S-coil and the modified S-kink estimators clearly exceed N as t increases. This apparently unplausible feature is due to the fact that the modified estimators only serve to provide an upper bound for N_e, while the unmodified versions provide a lower bound, as discussed in [65]. We observe that $\mathcal{N}_e^{\text{S-coil}}$ increases monotonically while $\mathcal{N}_e^{\text{S-kink}}$ first decreases and reaches a plateau after which it monotonically increases. Note that $\mathcal{N}_e^{\text{S-kink}}$ exceeds its equilibrium value at $t \approx 450$. Note that $\mathcal{N}_e^{\text{S-coil}}$ and $\mathcal{N}_e^{\text{S-kink}}$ reach the values 100 and 70, respectively, which are typical for chains of length 100 [33,34]. According to our previous analysis of entanglement, we expect that for $t < 150$, where $\mathcal{Z}$ increases, the length of the entanglement strands decreases, while for $t > 150$, N_e increases, as the number of entanglements decreases. This suggests that the tube gets thinner fast at first and after a characteristic time the tube disintegrates. We observe that $\mathcal{N}_e^{\text{S-kink}}$ is the only classical estimator that clearly agrees with the scaling of $\mathcal{Z}$.

Our data on the N_e-estimator based on writhe (Fig. 9) suggest that this estimator, when κ is replaced by varying stiffness $\kappa(t)$, gives values intermediate between the $\mathcal{N}_e^{\text{S-coil}}$ and $\mathcal{N}_e^{\text{S-kink}}$ estimators also in nonequilibrium. Moreover, for $t < 150$, we observe that the entanglement length decreases, as expected for a more entangled system, while it increases for $t > 150$, showing a jump to values greater than 100 at about $t \approx 700$. It is worth noticing that this estimator does not show a plateau as the $\mathcal{N}_e^{\text{S-kink}}$ estimator. It attains a minimum at the time $\mathcal{Z}$ reaches a maximum; furthermore the value of $\mathcal{N}_e^{\mathcal{W}_e^2}$ at $t \approx 300$ coincides with its equilibrium value.

E. The ACN

The ACN is the simplest measure of entanglement that has been most commonly used by mathematically inclined researchers to study entanglement in physical systems [47,52–55]. The ACN is very sensitive on the motion of the chains and on their length. The average $\langle \text{ACN} \rangle = \langle \text{ACN} \rangle$ taken over all chains in the melt decreases monotonically in time [Fig. 10(a)], with a change of slope at about $t \approx 150$. Overall, we observe that the stretching of the chains dominates the behavior of $\langle \text{ACN} \rangle$. Recall that the stretching of the chains also dominates over $\mathcal{Z}$ the behavior of $\mathcal{L}_{\text{PP}}$. Figure 10(b) shows the variation of $\langle \text{ACN} \rangle$ versus $\mathcal{L}_{\text{PP}}$ during the flow. We find that $\langle \text{ACN} \rangle$ decreases as $\mathcal{L}_{\text{PP}}$ increases almost linearly. Notice that a relation between the two measures is not expected at first since $\langle \text{ACN} \rangle$ concerns the original FENE chains, while $\mathcal{L}_{\text{PP}}$ concerns their PPs. However, both $\langle \text{ACN} \rangle$ and $\mathcal{L}_{\text{PP}}$ are measures of entanglement that depend on the geometry of the chains and are affected by the stretching of the chains and by the loss of kinks.

F. The writhe

The writhe is a measure of global self-entanglement of the chains, more informative than the ACN. However, it also depends on the particular configuration and changes with the motion of the chains. By combining the results of the Z1 algorithm with the writhe of the original FENE chains and the writhe of the corresponding PPs, we can examine separately the global self-entanglement of the chains, the global self-entanglement of their PPs, and the global self-entanglement of the entanglement strands.

1. The writhe of the original chains

Figures 11(a) and 11(b) show the transient behavior of the mean absolute writhe averaged over all chains in the melt. The

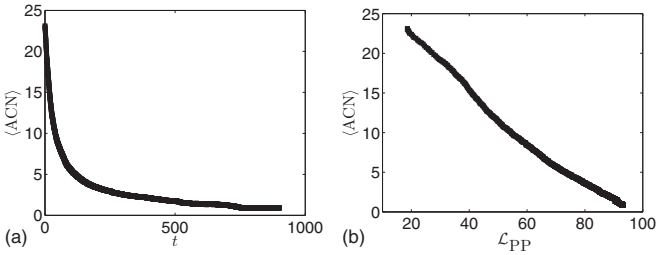

FIG. 10. (a) $\langle \text{ACN} \rangle$ vs time. (b) $\langle \text{ACN} \rangle$ vs $\mathcal{L}_{\text{PP}}$.

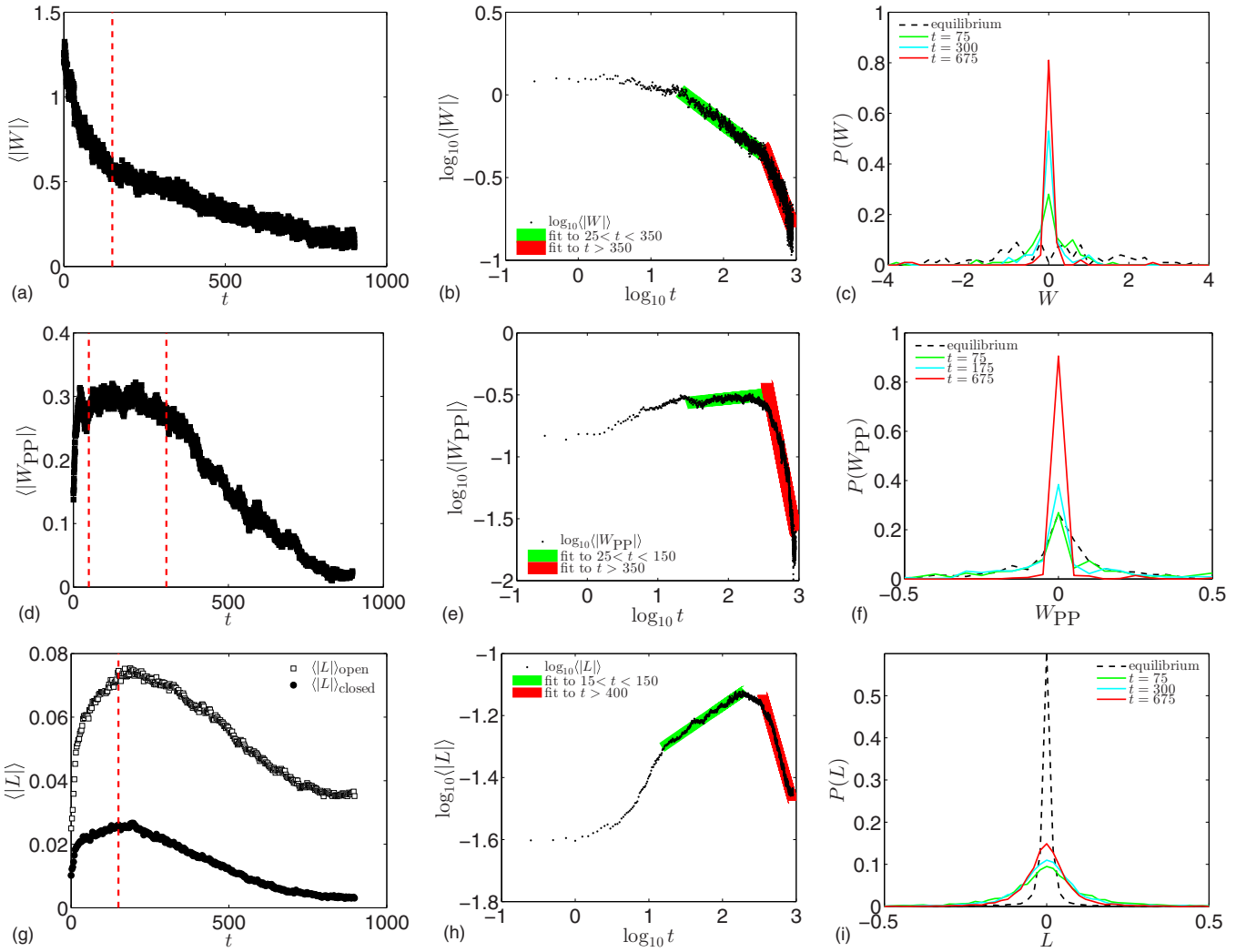

FIG. 11. (Color online) (a) Mean absolute writhe, $\langle|W|\rangle$ vs time. The vertical dashed line is at $t = 150$. (b) Corresponding double logarithmic plot. (c) Probability distribution of W in the course of time. (d) Mean absolute writhe of the PPs, $\langle|W_{\rm PP}|\rangle$ vs time. The two vertical dashed lines are at $t = 50$ and $t = 300$, respectively. (e) Corresponding double logarithmic plot. (f) Probability distribution of $W_{\rm PP}$. (g) Mean absolute linking number, $\langle|L|\rangle$ (vertical dashed line at $t = 150$). (h) Corresponding double logarithmic plot. (i) Probability distribution of L. We find $\langle|L|\rangle \approx 10^{-1.5} t^{0.16}$ for $t \in [15,150]$, $\langle|L|\rangle \approx 10^{-0.8} t^{-0.15}$ for $t \in [150,350]$, and $\langle|L|\rangle \approx 10^{1.1} t^{-0.86}$ for $t \in [400,700]$.

mean absolute writhe of the original FENE chains decreases monotonically with time. This is expected, since the chains stretch and the writhe gives on average smaller absolute value for more extended configurations [91]. We observe that the slope changes at $t \approx 150$, where the decrease weakens; the corresponding logarithmic plot reveals a possible additional crossover at $t \approx 450$.

The writhe and the number of kinks in a chain are not related in general, since a chain (in the original state) with $Z = 0$ (in its reduced state) may have the same writhe with a chain with $Z \neq 0$ (for an example, see [14]). The writhe can measure the global entanglement complexity of a conformation, while $\mathcal{Z}$ measures the number of contacts with other chains. However, one may expect that on average, the two measures follow a similar trend. For systems in equilibrium, a relationship between the number of kinks in a system of freely jointed chains of tangent hard spheres and the probability of knotting has been proposed. Specifically, it is conjectured that in equilibrium the population of entanglements and knots follow the same scaling laws at all volume fractions [41,42]. Moreover, in [14] it was shown that both the writhe and $\mathcal{Z}$ increased with N and it was shown that for the same systems at equilibrium the following relation holds:

$$\langle|W|\rangle \approx 1.245(\mathcal{Z} - 0.679)^{0.5} + 0.0504(\mathcal{Z} - 0.679)^{-0.5} - 0.5013. \quad (10)$$

Figures 12(a)and 12(b) show $\langle|W|\rangle$ with respect to $\mathcal{Z}$ for our chains in time under the action of a pulling force. Obviously, Eq. (10) does not hold when the chains are out of equilibrium. A deviation from relationships satisfied in equilibrium for chains subjected in flow had been observed recently [33]. For $t < 150$, as $\mathcal{Z}$ increases, $\langle|W|\rangle$ decreases and we observe an inverse linear relation, i.e., the number of kinks increases, while the global self-entanglement of a chain decreases. For $t < 150$ there are two competing effects to the writhe of the original chains. On one hand the increase of $\mathcal{Z}$ suggests that the conformations of the chains become more complex, which would

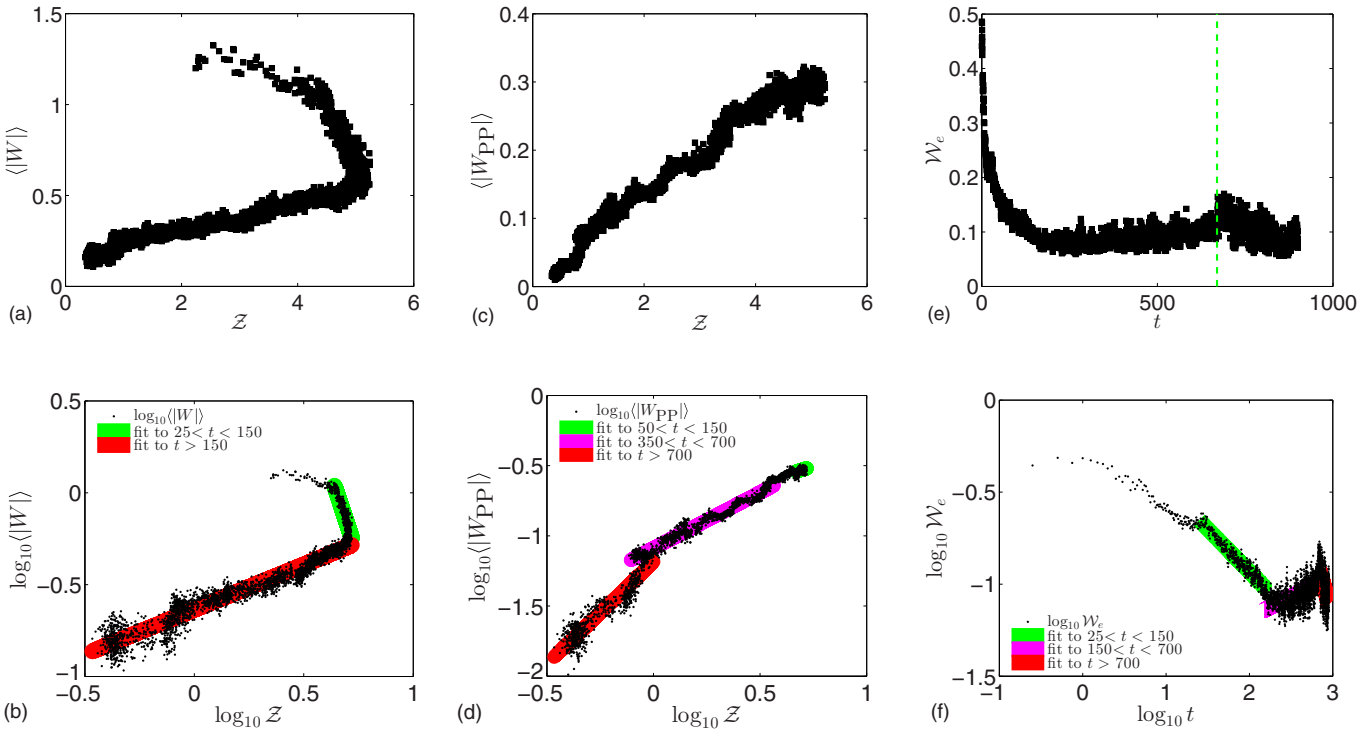

FIG. 12. (Color online) (a) Writhe versus $\mathcal{Z}$ and the (b) corresponding double logarithmic plot. We find $\langle|W|\rangle \approx 10^{2.34}\mathcal{Z}^{-3.59}$ for $t \in [25,150]$ and $\langle|W|\rangle \approx 10^{-0.64}\mathcal{Z}^{0.49}$ for $t > 150$. (c) Mean absolute writhe of the PP versus Z and (d) corresponding double logarithmic plot. We find $\langle|W_{PP}|\rangle \approx 10^{0.06}\mathcal{Z}^{-0.94}$ for $t \in [25,50]$, $\langle|W_{PP}|\rangle \approx 10^{-0.85}\mathcal{Z}^{0.45}$ for $t \in [50,150]$, $\langle|W_{PP}|\rangle \approx 10^{-0.89}\mathcal{Z}^{0.51}$ for $t \in [150,350]$, $\langle|W_{PP}|\rangle \approx 10^{-1.09}\mathcal{Z}^{0.79}$ for $t \in [350,700]$, and $\langle|W_{PP}|\rangle \approx 10^{-1.2}\mathcal{Z}^{1.46}$ for $t > 700$. (e) Mean writhe of an entanglement strand, $\mathcal{W}_e$. The line at $t \approx 700$ indicates the transition of $\mathcal{Z}$ to values $\mathcal{Z} < 1$. (f) Corresponding double logarithmic plot. We find $\mathcal{W}_e \approx 10^{0.005}\mathcal{Z}^{-0.46}$ for $t \in [25,150]$ and $\mathcal{W}_e \approx 10^{-1.64}\mathcal{Z}^{0.22}$ for $t > 150$.

tend to increase $\langle|W|\rangle$. On the other, the chains stretch out. The variation of the writhe indicates that the stretching of the chains has a more pronounced effect on the complexity of individual conformations. For $t > 150$ the two measures are similarly decreasing following a linear relation. It is interesting to remark that the crossovers are observed at integer values of $\mathcal{Z}$.

These results, and especially those for the $t < 150$ regime, clearly confirm that the two measures capture different entanglement information. The writhe is a measure of the global geometrical complexity of the chains, while the number of kinks is a local measure of topological constraints.

We further investigated the behavior of the probability distribution $P(W)$ [Fig. 11(c)]. In equilibrium, the distribution is Gaussian, which is consistent with previous analysis of linear polymer melts. But as the time increases, the $P(W)$ curves become asymmetric and more narrow around zero. This is consistent with the fact that $\langle|W|\rangle$ decreases with t. At $t > 600$, however, we observe that $P(W)$ exhibits small peaks at large values of W. This indicates that while most chains are not self-entangled at this time, there still exist some with nonvanishing writhe, such as chain B in Fig. 3 and all chains shown in Fig. 4(b).

2. *The writhe of the PPs*

The writhe of the PP is a quantity that characterizes the global geometrical/topological complexity of the PP. The writhe of the PP is expected to provide information about the motion of the surrounding tube. It is therefore of particular interest to compare it to that of the original chain. Moreover, the writhe of the PP in addition to Z, could provide further information on the nature of the kinks in a chain, i.e.. whether they are simple contacts, or they alter the topology of the conformation, possibly indicating the presence of persistent entanglements [14,92,93].

Figures 11(d)–11(f) show the transient behavior of the mean absolute writhe of all PPs in the PP network obtained by the application of the Z1 algorithm. For a short duration after the onset of the pulling force the mean absolute writhe of the PPs increases monotonically, to reach a plateau at $t \approx 50$. For $t < 300$, $\langle|W_{PP}|\rangle$ fluctuates around the constant value 0.3. $\langle|W_{PP}|\rangle$ starts to decrease at $t \approx 300$ and slows down after $t > 750$. Importantly, the increase of $\langle|W_{PP}|\rangle$ for $t < 50$ and the decrease for $t > 300$ is in accordance with the behavior of $\mathcal{Z}$ in the same time intervals. Figure 12(c) shows the variation of the writhe of the PP with respect to $\mathcal{Z}$. The data are very well represented by a linear relation. This relation is similar to the one that had been reported in equilibrium [14]. The corresponding double logarithmic plot [Fig. 12(d)] resolves several crossovers. In point of fact, for $t < 25$ the writhe increases as expected for a coil of an increasing number of edges. This indicates that the created entanglements are not all simple contacts, but that the conformations of the PPs get indeed more complex. At $t \approx 50$ $\langle|W_{PP}|\rangle$ drops quickly to a local minimum [visible in Figs. 11(e) and (6)b, less visible in Fig. 12(c) because of the re=entrance at larger t],

something that has no analog in the behavior of $\mathcal{Z}$. Furthermore we observe that for $50 < t < 300$ $\langle|W_{PP}|\rangle$ is almost constant while $\mathcal{Z}$ increases. At $t > 50$, the mean absolute writhe of the PP returns to its value at $t \approx 25$ and remains almost constant up to $t \approx 150$, while $\mathcal{Z}$ continuously increases in this time. Thus, $\langle|W_{PP}|\rangle$ deviates from the writhe of a random coil of $\mathcal{Z}+1$ edges in the interval $50 \leqslant t \leqslant 300$. In other words, the creation of new kinks in this interval does not affect the global self-entanglement of the PPs. Our results thus demonstrate that only a portion of the newly created entanglements under tension contribute to a more complex global conformation of the tube. It might be interesting to examine if the overshoot in viscosity for polymer melts after startup of flow relates to only the portion of newly created entanglements, which are related to the global entanglement of the tube. We observe that $\langle|W_{PP}(150)|\rangle \approx 2\langle|W_{PP}(0)|\rangle$, while $\mathcal{Z}(150) \approx 2.5\mathcal{Z}(0)$. Also, we find pronounced discontinuities at $\mathcal{Z} \approx 4,3,2$. This indicates that the writhe of the PP shows a crossover when a kink is lost, which suggests a fast rearrangement of the configuration to a more linear one. At $t \approx 450$ the quantities $\langle|W_{PP}(450)|\rangle$ and $\langle|W_{PP}(0)|\rangle$ are approximately equal, in analogy with the case of $\mathcal{Z}$.

It is worth emphasizing that the behaviors of $\langle|W|\rangle$ and $\langle|W_{PP}|\rangle$ differ substantially. For $t < 150$, $\langle|W|\rangle$ decreases while $\langle|W_{PP}|\rangle$ increases. This indicates that the chains continuously stretch out while the tube gets more entangled. For $t < 350$, $\langle|W|\rangle$ decreases while $\langle|W_{PP}|\rangle$ is almost constant. During that period, the chains continue being stretched while the tube remains in an unaltered conformation. For $t > 450$ both $\langle|W|\rangle$ and $\langle|W_{PP}|\rangle$ follow the same scaling, both decreasing. Interestingly, $\langle|W(t)|\rangle > \langle|W_{PP}(t)|\rangle$, for all t. This suggests that even at large t, when the PPs have stretched out, chains have eventually not stretched out in a comparable fashion due to self-entanglement or knotting of the original chains (chain B in Fig. 3 and also chains shown in Fig. 4).

Our NEMD results for the probability distribution of $P(W_{PP})$ of the number of entanglements as a function of time are shown in Fig. 11(f). At equilibrium, the distribution is Gaussian, which is consistent with previous analysis of linear polymer melts. $P(W_{PP})$ follows a less symmetric distribution at larger t, and as time proceeds further, the $P(W_{PP})$ curves become more narrow, reflecting the pathway towards unentangled PPs.

3. *The writhe of the entanglement strands*

Next we characterize the writhe of the entanglement strands. This measure provides further information on the disentanglement process of the chains, at a length scale that has not been discussed so far.

In [14] a method to estimate the mean writhe of an entanglement strand had been introduced:

$$\mathcal{W}_e = \left\langle \frac{\sum_{i=1}^{Z+1} W(e_i)}{Z+1} \right\rangle = \left\langle \frac{W(I) - W_{PP}(I)}{Z+1} \right\rangle, \qquad (11)$$

where I denotes a chain in the melt, $W(I)$ denotes its writhe, $W_{PP}(I)$ the writhe of the corresponding reduced chain, and $e_i, i = 1, \ldots, Z+1$ denote the entanglement strands in I. The mean squared writhe of an entanglement strand is given by [14]

$$\mathcal{W}_e^2 \approx \left\langle \frac{[W(I) - W_{PP}(I)]^2}{Z+1} \right\rangle. \qquad (12)$$

We stress that these are semianalytical formulas and for their computation only the writhe of the original and reduced chains is used, and $\mathcal{Z}$. The definition (12) relates only indirectly parts of the chains between entanglements to entanglement strands. Both Eqs. (11) and (12) hold for chains both in equilibrium and nonequilibrium. Still, under nonequilibrium conditions, there may be a significant deviation of the writhe of an entanglement strand from this average, since the assumption underlying Eq. (12) that all the entanglement strands are similar may no longer hold. Recall that both $\mathcal{W}_e$ and $\mathcal{W}_e^2$ vanish by definition for rodlike polymers, where $W = W_{PP} = Z = 0$. On the other hand, when the polymer chains inside a rodlike tube are not fully elongated, i.e., when $W_{PP} = Z = 0$, but $W \neq 0$, then $\mathcal{W}_e, \mathcal{W}_e^2$ are nonzero and they equal W and W^2, respectively.

The results of our data are shown in Figs. 12(e) and 12(f). We observe that $\mathcal{W}_e$ and $\mathcal{W}_e^2$ both decrease monotonically for $t \leqslant 150$. Next, they show a small increase for $t < 700$. At $t \approx 700$, however, we observe a jump to a larger value and then for $t > 700$, they decrease continuously. Obviously, as the chains stretch the entanglement strands must stretch as well, and thus their writhe decreases. Moreover, for $t < 150$ the PPs get more entangled and as the number of entanglements increases, the length of the entanglement strands decreases and thus their writhe decreases to that of a coil of smaller length. At times $t > 150$, the chains disentangle, since both $\mathcal{Z}$ and W, W_{PP} decrease and $\mathcal{R}_{ee}$ increases slowly, which is strongly supported by our data. But we observe that the writhe of the entanglement strands remains almost constant at $W_{PP}(150)$. Again there may be two competing effects: As $\mathcal{Z}$ decreases the length of the entanglement strands increases causing an increase to the writhe of an entanglement strand, as a longer coil. On the other hand, as the chains continue to stretch, the writhe of the entanglement strand decreases. Moreover, we find that $\mathcal{W}_e$ shows several peaks at $t \approx 450$ and $t \approx 700$ which coincide with the decrease of $\mathcal{Z}$ below its integer values. These suggest that in the destruction of a kink, the new entanglement strand that is created has only a small amount of writhe, which gets reduced as the entanglement strand stretches out fast. Interestingly, for $t > 500$, $W_{PP}(t) < \mathcal{W}_e(t)$. This inequality indicates that when the PPs are almost stretched, the entanglement strands have still not stretched out. Consequently, the chains contain knots at the level of entanglement strands.

The writhe of the entanglement strands reaches a plateau value at $t \approx 200$ and thus shows very different behavior compared with the writhe of the PPs. This suggests that newly created entanglements contain entanglement strands different from those created in equilibrium. They are less twisted, more extended, and they straighten further when the PP straightens.

The observed discontinuity at $t \approx 700$ is absent in $\mathcal{Z}$, $\langle|W|\rangle$, and $\langle|W_{PP}|\rangle$. This may signal the complete destruction of the tube. Notice that at $t \approx 700$, $\mathcal{Z} = 1$, and the chains are getting close to rodlike polymers ($Z = 0$). In this limit the writhe of an entanglement strand by definition [Eq. (11)] equals

$W(I) - W_{\mathrm{PP}}$. Inspecting our values for $\langle|W|\rangle$, $\langle|W_{\mathrm{PP}}(I)|\rangle$, and $\mathcal{W}_e$, this is perfectly confirmed.

G. The linking number

So far we discussed the entanglement properties of individual chains. Next, we examine the linking number, being a measure of pairwise entanglement. To this end we are going to focus on the mean absolute linking number of a pair of chains in a melt and that of the corresponding end-to-end closed chains. We recall that for open chains the linking number is a continuous function in the space of configurations and it may be nonzero even for chains whose topological cells are disjoint, giving smaller values with increasing distance of the chains centers of mass. For closed chains it is an integer topological invariant that can resolve different link types up to link homotopy, and it is exactly equal to zero for chains that are unlinked.

Figure 13(a) shows the mean absolute linking number, $\langle|L|\rangle$, of the chains in time. We observe that for $t < 150$, $\langle|L|\rangle$ increases and reaches a plateau value and remains almost constant for all $t > 150$. There are two factors that can contribute to the increase of $|L|$: the decrease in the distance of each pair of chains and the increase of the entanglement complexity. Our previous analysis suggests that for $t < 150$ the chains stretch out and create more contacts with other chains. Correspondingly, for $t < 150$, we observe a fast increase of the mean absolute linking number, while there are two competing

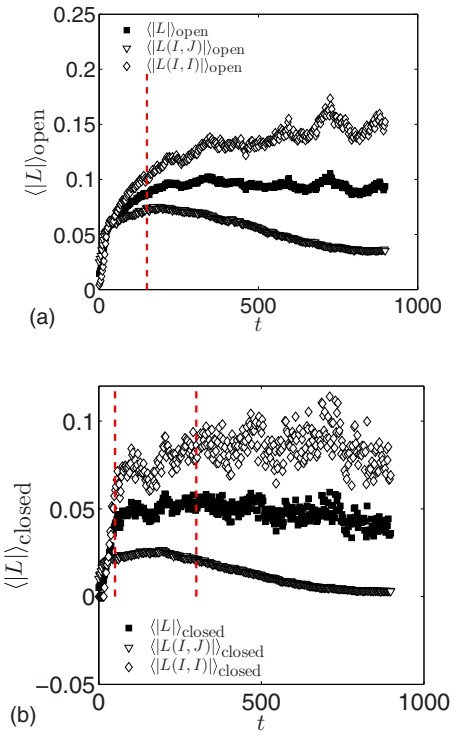

FIG. 13. (Color online) (a) Mean absolute linking number of the original chains with all surrounding chains (black squares), with images of other chains (white triangles) and with self-images (white diamonds). The vertical dashed line corresponds to $t = 150$. (b) Same as (a) for the corresponding end-to-end closed chains, and vertical dashed lines at $t = 50$ and $t = 300$.

effects for $t > 150$: The chains disentangle, thus their linking number should decrease, but as they stretch out, they also get closer—accompanied by an increase of the linking number. Above we demonstrated already that the chains exhibit only a small writhe. The indicated collapsed structures of chains suggest that contacts with other chains can be only with chains whose center of mass is close by. Due to the periodicity of the system, the chains in the vicinity will mostly be translations of the same image. Thus in the following we will determine the chains in the vicinity of a chain, say I, by exactly the periodic images of I that intersect the cells in which I unfolds. The same Fig. 13(a) shows separately the mean absolute linking number of a chain with images of the other chains, denoted as $|L(I,J)|$, and the mean absolute linking number of a chain with its own images, denoted by $|L(I,I)|$. Both quantities increase in a similar fashion only up to $t \approx 50$.

The mean absolute linking number over images of other chains, $\langle|L(I,J)|\rangle$, reaches its maximum at $t \approx 150$ and subsequently decreases almost monotonically, reminiscent of the behavior we observed for $\mathcal{Z}$ and the mean absolute writhe of the PPs. This type of behavior, characteristic for the present setup, suggests that the information captured by $\mathcal{Z}$ may be related to the linking number of the original chains with images of other chains. We observe that $\langle|L(I,J)(150)|\rangle \approx 3\langle|L(I,J)(0)|\rangle$, to be compared with $\mathcal{Z}(150) \approx 2.5\mathcal{Z}(0)$ and $\langle|W_{\mathrm{PP}}(150)|\rangle \approx 2\langle|W_{\mathrm{PP}}(0)|\rangle$. It is worth remarking that the probability distribution of $L(I,J)$ [Fig. 11(i)] is Gaussian for all t and does not show a significant distortion from that shape for $t > 600$, as was observed for the writhe of the PPs.

On the other hand, $|L(I,I)|$, the mean absolute linking number with self-images, increases for all t. This suggests that, even when the entanglements are lost, the decrease of the distance between a chain and the chains in its vicinity has a more pronounced effect to their linking. Notice that if all chain contours were parallel, $L(I,I)$ would vanish, but our data indicate that the chains do not attain parallel conformations, in accordance to our finding $\langle|W(t = 900)|\rangle \neq 0$.

Figure 13(b) shows the mean absolute linking number of the closed chains that result by direct end-to-end closure of all the chains in the melt (black squares). The linking number of closed chains is a topological invariant; it remains unchanged if the chains are not allowed to cross each other. However, here we examine the end-to-end closed chains at each time step and not physical ring polymers, so we expect their linking number to change in time, but the corresponding value now is indicative of different link types, and it is exactly zero for unlinked chains. Again, we observe an increase of the mean absolute linking over all surrounding chains and a different behavior for the linking with images of others than that of the linking with self-images. First of all, the average absolute value of the linking number increases for $t < 50$ and remains almost constant for $t > 50$. This suggests that the increase observed in the mean absolute linking number of the original chains is not an effect of the tightening of the pairwise configurations, but shows that the new entanglements change the topology. For $t > 50$, the linking with chains in its vicinity (linking with self-images) increases to a greater value and reaches a plateau. This is caused by the fact that the chains in the vicinity are not completely aligned, thus showing this nontrivial linking. While both quantities increase up to $t \approx 50$, for $50 < t < 300$,

we observe that $\langle |L| \rangle$ is constant. This indicates that only a portion of $\mathcal{Z}$ alters the topology of the melt in a large scale and that the rest of the topological constraints are only simple contacts with chains in the vicinity. Note that a similar conclusion derives from the analysis of $W_{\rm PP}$. For $t > 300$ the mean absolute linking number of the end-to-end closed chains with images of other chains tends to zero.

H. The linking matrix—Effect on homogeneity

Here we employ the linking matrix to test the homogeneity of the global pairwise entanglement in the system. Spatial inhomogeneities had been discussed earlier in the context of elongational flow for the FENE polymer melts [8].

Figure 14(a) shows the average second smallest eigenvalue λ_2 of the Laplacian of the periodic linking matrix, which is related to the vertex expansion of the periodic linking graph; it takes larger values for "well-connected" graphs. Recall that λ_2 is related to the Cheeger constant h_G by the inequality $2h_G \geqslant \lambda_2 \geqslant h_G^2/2$. Our results suggest that $0.3 \leqslant h_G \leqslant 1$ for all t. This measure reveals that the upper and lower bounds of the homogeneity of the global pairwise entanglement for the original open chains is almost constant, showing a small tendency for an initial decrease of global entanglement inhomogeneity, to be compared with an observed small increase of local spatial inhomogeneity reported in [8]. Similarly, the averaged maximum eigenvalue $\lambda_{\rm max}$ of the Laplacian of the linking matrix does not exhibit dramatic changes [Fig. 14(b)].

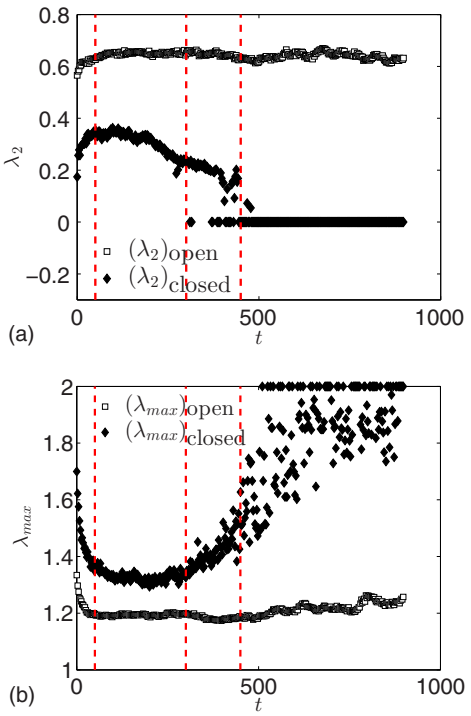

FIG. 14. (Color online) (a) The mean second smallest eigenvalue λ_2 of the Laplacian of the [inking matrix of open (squares) and end-to-end closed (diamonds) chains. (b) The maximum eigenvalue $\lambda_{\rm max}$ of the Laplacian of the periodic linking matrix for open (squares) and end-to-end closed (diamonds) chains. Vertical dashed lines are drawn at $t = 50$, $t = 300$, and $t = 450$.

The underlying reason for the overshoot is that the chains get entangled with more chains as they stretch out. For $t > 150$, we observe that the homogeneity remains constant, while the chains disentangle. This counterintuitive result is probably due to the increased linking of chains with chains in their vicinity.

A different behavior we observe for $\langle \lambda_2 \rangle$ and $\langle \lambda_{\rm max} \rangle$ of the Laplacian of the linking matrix of the corresponding end-to-end closed chains [Figs. 14(a) and 14(b)]. Our results indicate that the global linking inhomogeneity increases for $t > 150$. Moreover, at $t \approx 300$ we find that λ_2 attains the value 0 for the first time, representing a disconnected system, and showing that there exist collections (clusters) of chains that are entangled with chains from the same collection, but not with chains from other collections. For all $t > 450$, $\lambda_2(t)$ identically vanishes. On the other hand $\lambda_{\rm max}$ increases for $t > 300$ and for $t > 450$ the $\langle \lambda_{\rm max} \rangle$ approaches 2 with time, which is the value that corresponds to a completely disconnected system [72]. Actually, this is expected, since the linking number of closed chains exactly vanishes for unlinked chains. As the chains disentangle, the end-to-end closed chains in the vicinity of a chain are linked with it, while the rest is not, implying that chains are preferentially arranged in disconnected layers.

V. CONCLUSIONS

Overall we conclude that the degree of chain entanglement is affected by the imposed external force in a rather complicated way due to effects associated with chain extension, which tends to initially create more entanglements, and chain alignment, that acts in the opposite direction. Results are thus affected by differences in local and global alignment [8]. On the basis of the results shown here, the extension effect dominates alignment up to $t < 150$, i.e., after having traveled over a distance of about 40 bond lengths, beyond which the situation is reversed.

We find that both $\mathcal{Z}$ and $\langle |L| \rangle_{\rm open}$ increase up to their maximum values at $t \approx 150$ clearly signaling that the PPs get more entangled with each other during a relevant fraction of the pulling experiment. Our results for $\langle |W_{\rm PP}| \rangle$ and $\langle |L| \rangle_{\rm closed}$ reveal that during the early phase, $t < 50$, chains do not only create more contacts with each other, but also alter the topology of the melt. However, during an intermediate stage, $50 < t < 150$, the newly created entanglements do not increase the entanglement complexity of the melt. At large times, $t > 150$, the amount of entanglement decreases continuously and ultimately tends to result in conformations of trivial linking.

Results we obtained for $\mathcal{R}_{\rm ee}$, $\mathcal{L}_{\rm PP}$, $\langle$ACN$\rangle$, $\langle |W| \rangle$, and $\mathcal{W}_e$ indicate that all these quantities vary monotonically in the course of time, changing slope at $t \approx 150$. At times $t < 150$ the chain extension dominates the creation of more entanglements. We observe an affine transformation of chain dimensions and our results on $\langle |W| \rangle$, $\langle |W_{\rm PP}| \rangle$, and $\mathcal{W}_e$ highlight that the stretching of the chains at $t < 150$ occurs at the level of entanglement strands. At $t > 150$, where the disentanglement of the PPs sets in, the entanglement strands continue to stretch more slowly, without reaching a fully disentangled state, which may suggest the presence of local knots [94].

Our measurements of N_e imply that the tube disintegrates in time during the pulling experiment. The N_e estimators based on

kinks and coils give different results at each time with the latter being almost twice as large as the former. We have introduced a method to compute the N_e estimator based on writhe and we find that it gives values intermediate between the $\mathcal{N}_e^{\text{S-coil}}$ and $\mathcal{N}_e^{\text{S-kink}}$ estimators also in nonequilibrium. Moreover, our results show that the new entanglements increase the system's global entanglement homogeneity, as the chains have only a very small linking with all the chains in the melt.

Having chosen a setup that allows one to vary the amount of entanglement very quickly, compared with a more conventional and time-demanding nonequilibrium study, and in contrast with an equilibrium study that needs to extract information from fluctuations only, this work sheds light on the relationship between quantities that characterize different conformational and topological aspects of a melt of linear polymer chains all the way from maximally entangled to unentangled or a tight knot. Results presented here may provide insight to future experiments involving optical tweezers or magnetic molecules that allow one to transmit a force to individual monomers embedded in an entangled polymeric system.

Note added. Recently it came to our attention that a slightly different setup than ours (application of opposing constant forces to end beads in a polymer melt) had been studied by Qin and Milner [95].

ACKNOWLEDGEMENT

This research was supported by Swiss Government Scholarship No. 2011.0409

[1] M. Doi and S. F. Edwards, *The Theory of Polymer Dynamics* (Clarendon, Oxford, 1986).
[2] P. G. de Gennes, *Scaling Concepts in Polymer Physics* (Cornell University Press, New York, 1979).
[3] M. Rubinstein and E. J. Helfand, J. Chem. Phys. **82**, 2477 (1985).
[4] T. Murashima and T. Tanigushi, Europhys. Lett. **96**, 18002 (2011).
[5] Y. Li, B. C. Abberton, M. Kröger, and W. K. Liu, Polymers **5**, 751 (2013).
[6] D. E. Smith and S. Chu, Science **281**, 1335 (1998).
[7] J. P. Gao and J. H. Weiner, Macromolecules **29**, 6048 (1996).
[8] M. Kröger, C. Luap, and R. Muller, Macromolecules **30**, 526 (1997).
[9] D. W. Mead, R. G. Larson, and M. Doi, Macromolecules **31**, 7895 (1998).
[10] M. Kröger and S. Hess, Phys. Rev. Lett. **85**, 1128 (2000).
[11] G. Marrucci and G. Iannniruberto, Macromolecules **37**, 3934 (2004).
[12] P. Ilg, H. C. Öttinger, and M. Kröger, Phys. Rev. E **79**, 011802 (2009).
[13] M. Harasim, B. Wunderlich, O. Peleg, M. Kröger, and A. R. Bausch, Phys. Rev. Lett. **110**, 108302 (2013).
[14] E. Panagiotou, M. Kröger, and K. C. Millett, Phys. Rev. E **88**, 062604 (2013).
[15] R. Everaers, S. K. Sukumaran, G. S. Grest, C. Svaneborg, A. Sivasubramanian, and K. Kremer, Science **303**, 823 (2004).
[16] M. Kröger, Comput. Phys. Commun. **168**, 209 (2005).
[17] C. Tzoumanekas and D. N. Theodorou, Macromolecules **39**, 4592 (2006).
[18] S. Shanbhag and M. Kröger, Macromolecules **40**, 2897 (2007).
[19] M. Kröger, J. Ramirez, and H. C. Öttinger, Polymer **43**, 477 (2002).
[20] M. Kröger and H. Voigt, Macromol. Theory Simul. **3**, 639 (1994).
[21] J. Qin and S. T. Milner, Soft Matter **7**, 10676 (2011).
[22] Z1 is available online at http://www.complexfluids.ethz.ch/Z1.
[23] N. C. Karayiannis and M. Kröger, Int. J. Mol. Sci. **10**, 5054 (2009).
[24] S. K. Sukumaran, G. S. Grest, K. Kremer, and R. Everaers, J. Polym. Sci., Part B: Polym. Phys. **43**, 917 (2005).
[25] Q. Zhou and R. G. Larson, Macromolecules **38**, 5761 (2005).
[26] S. Shanbhag and R. G. Larson, Phys. Rev. Lett. **94**, 076001 (2005).
[27] K. Foteinopoulou, N. C. Karayiannis, V. G. Mavrantzas, and M. Kröger, Macromolecules **39**, 4207 (2006).
[28] S. Shanbhag and R. G. Larson, Macromolecules **39**, 2413 (2006).
[29] P. S. Stephanou, C. Baig, G. Tsolou, V. G. Mavrantzas, and M. Kröger, J. Chem. Phys. **132**, 124904 (2010).
[30] Y. Y. Wang, S. W. Cheng, and S. Q. Wang, J. Rheol. **55**, 1247 (2011).
[31] J. M. Rallison and E. J. Hinch, J. Non-Newtonian Fluid Mech. **29**, 37 (1988).
[32] R. G. Larson, Rheol. Acta **29**, 371 (1990).
[33] C. Baig, V. G. Mavrantzas, and M. Kröger, Macromolecules **43**, 6886 (2010).
[34] J. M. Kim, D. J. Keffer, M. Kröger, and B. J. Edwards, J. Non-Newtonian Fluid Mech. **152**, 168 (2008).
[35] Y. Li, S. Tang, B. C. Abberton, M. Kröger, C. Burkhart, B. Jiang, G. J. Papakonstantopoulos, M. Poldneff, and W. K. Liu, Polymer **53**, 5935 (2012).
[36] D. Kivotides, S. L. Wilkin, and T. G. Theofanous, Phys. Rev. E **80**, 041808 (2009).
[37] P. Freyd, D. Yetter, J. Hoste, W. Lickorish, K. Millett, and A. Ocneanu, Bull. Am. Math. Soc. **12**, 239 (1985).
[38] J. Przytycki and P. Traczyk, Proc. Am Math. Soc. **100**, 744 (1987).
[39] L. H. Kauffmann, *Knots and Physics*, Series on Knots and Everything Vol. 1 (World Scientific, Singapore, 1991).
[40] E. Panagiotou, T Ph.D. thesis, National Technical University of Athens, 2012.
[41] K. Foteinopoulou, N. Ch. Karayiannis, M. Laso, M. Kröger, and M. L. Mansfield, Phys. Rev. Lett. **101**, 265702 (2008).
[42] M. Laso, N. C. Karayiannis, K. Foteinopoulou, L. Mansfield, and M. Kröger, Soft Matter **5**, 1762 (2009).
[43] K. Millett, A. Dobay, and A. Stasiak, Macromolecules **38**, 601 (2005).
[44] J. I. Sulkowska, E. J. Rawdon, K. C. Millett, J. N. Onuchic, and A. Stasiak, Proc. Natl. Acad. Sci. USA **109**, E1715 (2012).
[45] L. Tubiana, A. Rosa, F. Fragiacomo, and C. Micheletti, Macromolecules **46**, 3669 (2013).

[46] P. K. Agarwal, H. Edelsbrunner, and W. Y., Discrete Comput. Geom. **32**, 37 (2004).
[47] Y. Diao, A. Dobay, and A. Stasiak, J. Phys. A: Math. Gen. **38**, 7601 (2005).
[48] K. Klenin and J. Langowski, Biopolymers **54**, 307 (2000).
[49] M. A. Berger and C. Prior, J. Phys. A. **39**, 8321 (2006).
[50] C. Laing and D. W. Sumners, J. Phys. A **39**, 3535 (2006).
[51] C. Laing and D. W. Sumners, J. Knot Theor. Ramif. **17**, 1575 (2008).
[52] J. Arsuaga, Y. Diao, and M. Vazquez, *in Mathematics of DNA Structure, Function and Interactions*, edited by C. J. Benham, S. Harvey, W. K. Olson, D. W. Sumners, and D. Swigon (Springer Science + Business Media, New York, 2009), p. 7.
[53] G. A. Arteca, Phys. Rev. E. **56**, 4516 (1997).
[54] G. A. Arteca and O. Tapia, Int. J. Quantum Chem. **80**, 848 (2000).
[55] Y. Diao, R. N. Kushner, K. Millett, and A. Stasiak, J. Phys. A: Math. Gen. **36**, 11561 (2003).
[56] A. Abedijaberi, J. Soulages, M. Kröger, and B. Khomami, Rheol. Acta **48**, 97 (2009).
[57] S. P. Singh, D. A. Fedosov, A. Chatterji, R. G. Winkler, and G. Gompper, J. Phys: Condens. Matter **24**, 464103 (2012).
[58] G. N. Toepperwein, N. C. Karayiannis, R. A. Riggleman, M. Kröger, and J. J. de Pablo, Macromolecules **44**, 1034 (2011).
[59] Y. Li, M. Kröger, and W. K. Liu, Macromolecules **45**, 2099 (2012).
[60] A. Gupta and M. Gupta, Biomaterials **26**, 3995 (2005).
[61] B. Gleich and J. Weizenecker, Nature (London) **435**, 1214 (2005).
[62] K. Scarberyy, E. Dickerson, J. McDonald, and J. Zhang, J. Am. Chem. Soc. **130**, 10258 (2008).
[63] G. Gnanaprakash, S. Ayyappan, T. Jayakumar, J. Phillip, and B. Raj, Nanotechnology **17**, 5851 (2006).
[64] I. Rabias, D. Tsitrouli, E. Karakosta, G. Diamantopoulos, M. Fardis, D. Stamopoulos, T. Maris, P. Falaras, N. Zouridakis, N. Diamantis *et al.*, Biomicrofluidics **4**, 024111 (2010).
[65] R. S. Hoy, K. Foteinopoulou, and M. Kröger, Phys. Rev. E **80**, 031803 (2009).
[66] K. Foteinopoulou, N. C. Karayiannis, M. Laso, and M. Kröger, J. Phys. Chem. B **113**, 442 (2009).
[67] J. D. Schieber, J. Chem. Phys. **118**, 5162 (2003).
[68] F. Lahmar, C. Tzoumanekas, D. N. Theodorou, and B. Rousseau, Macromolecules **42**, 7485 (2009).
[69] K. F. Gauss, *Werke* (Kgl. Gesellsch. Wiss. Göttingen, Göttingen, 1877).
[70] E. Panagiotou, C. Tzoumanekas, S. Lambropoulou, K. C. Millett, and D. N. Theodorou, Prog. Theor. Phys. Suppl. **191**, 172 (2011).
[71] E. Panagiotou, K. C. Millett, and S. Lambropoulou, Procedia IUTAM: Top. Fluid Dyn. **7**, 251 (2013).
[72] A. E. Brouwer and W. H. Haemers, *Spectra of Graphs*, Universitext Vol. XIV (Springer, New York, 2012).
[73] M. Kröger, W. Loose, and S. Hess, J. Rheol. **37**, 1057 (1993).
[74] Reduced Lennard-Jones units—online interactive tool available at http://polyphys-s01.ethz.ch/cgi-bin/units
[75] M. Kröger, Phys. Rep. **390**, 453 (2004).
[76] J. Portillo, Y. Diao, R. Scharein, J. Arsuaga, and M. Vazquez, J. Phys. A: Math. Theor. **44**, 275004 (2011).
[77] S. Sato, Y. Harada, and Y. Waseda, Opt. Lett. **19**, 1807 (1994).
[78] D. G. Grier, Nature (London) **424**, 810 (2003).
[79] D. H. King and D. F. James, J. Chem. Phys. **78**, 4749 (1983).
[80] G. Ryskin, J. Fluid. Mech. **178**, 423 (1987).
[81] C. Baig and V. G. Mavrantzas, J. Chem. Phys. **132**, 014904 (2010).
[82] C. Baig and V. G. Mavrantzas, Phys. Rev. B **79**, 144302 (2009).
[83] J. M. Kim, B. J. Edwards, D. J. Keffer, and B. Khomami, Phys. Rev. Lett. A **373**, 769 (2009).
[84] C. Aust, S. Hess, and M. Kröger, Macromolecules **35**, 8621 (2002).
[85] P. J. Daivis, M. L. Matin, and B. D. Todd, J. Non-Newtonian Fluid Mech. **111**, 1 (2003).
[86] J. Fang, M. Kröger, and H. C. Öttinger, J. Rheol. **44**, 1293 (2000).
[87] G. Marrucci, J. Polym. Sci. B **23**, 159 (1985).
[88] G. Marrucci, J. Non-Newtonian Fluid. Mech. **62**, 279 (1996).
[89] D. M. Sussman, W.-S. Tung, K. I. Winey, K. S. Schweizer, and R. A. Riggleman, Macromolecules Macromolecules **47**, 6462 (2014).
[90] R. Everaers, Phys. Rev. E **86**, 022801 (2012).
[91] E. J. Rawdon, J. C. Kern, M. Piatek, P. Plunkett, A. Stasiak, and K. C. Millett, Macromolecules **41**, 8281 (2008).
[92] S. Anogiannakis, C. Tzoumanekas, and D. N. Theodorou, Macromolecules **45**, 9475 (2012).
[93] D. G. Tsalikis, T. Koukoulas, and V. G. Mavrantzas, React. Funct. Polym. **80**, 61 (2014).
[94] J. Cantarella, A. LaPointe, and E. J. Rawdon, J. Phys. A: Math. Theor. **45**, 225202 (2012).
[95] J. Qin and S. T. Milner, Macromolecules **46**, 1659 (2013).